Large Strain Behaviour of Polycarbonate

J.G.A. van Houten

EUT, Faculty of Mechanical Engineering
Report No. WFW 94.108

Stage verslag

Coaches: dr.ir. L.E. Govaert
ir. R.J.M. Smit

Eindhoven, August 1994

Eindhoven University of Technology (EUT)
Faculty of Mechanical Engineering
Department of Fundamentals of Mechanical Engineering

Contents

Chapter 1

Introduction

Large strain behaviour of glassy polymers occurs at macroscale in many industrial solid phase forming processes, and even at microscale, for example at crack tips of ductile polymers but also at crack tips of macroscopically brittle polymers. For the prediction of these large deformations, nowadays usually with the aid of finite element calculations, reliable constitutive equations are necessary. In order to perform numerical simulations which accurately fit experimental data accurate material parameters and physical constants are necessary, besides exact constitutive equations. Especially the material parameters and physical constants which strongly influence the large strain behaviour. The large strain behaviour is dominated by a strain hardening effect due to orientation of the molecular network. The strain hardening effect is often described with the rubber elasticity theory, however, with varying success. Accurate material parameters and physical constants can only be obtained by applying appropriate formulas to appropriate experiments.

In this paper Gaussian strain hardening will be assumed to estimate a characteristic rubber elasticity parameter, the so-called strain hardening modulus G_p, from experimental engineering stress-strain curves. The investigation of the stress-strain behaviour is complicated by the formation of a neck, but in section 2.1 a formula derived by Haward [7,8] will be outlined, which relates the engineering stress σ_{Eng} and the natural draw ratio λ_D in the stabilized neck to the strain hardening modulus G_p:

$$G_p = \sigma_{Eng} \left(\frac{1 - \frac{1}{\lambda_D}}{\lambda_D - \frac{1}{\lambda_D{}^2}} \right)$$

The so obtained strain hardening modulus G_p could be used as an estimation for the equivalent Gaussian strain hardening modulus G_w used in a finite element implementation of the compressible Leonov model. In order to check if the formula gives a good estimation of G_w, the formula is applied to stress-strain curves derived by numerical simulations with the compressible Leonov model.

Chapter 2

Constitutive equations

During the last decades several different constitutive equations have been derived to describe the large strain behaviour of glassy polymers. Glassy polymers exhibit a non-linear elasto-viscoplastic nature, combined with strain hardening at large deformations and thermal effects. The strain hardening, which dominates the large strain behaviour, has shown to be the most difficult element to model. Therefore more attention is payed to the strain hardening element in the constitutive equations to be outlined. The strain hardening is often regarded as an entropy-effect and described with the rubber elasticity theory. One of the first one-dimensional equations was based on the Langevin function for rubber elasticity at high strains [12]. Later, more simple one-dimensional rubber elasticity equations have been found which give even better results, for example the Gaussian equation [9] and the Rivlin-Mooney equation [2]. Recently, more advanced three-dimensional constitutive equations have been developed, for example a so-called eight-chain non-Gaussian network which is based on a Langevin function [1], and a Gaussian equation [11]. Both three-dimensional equations are combined with a compressible Leonov model and implemented in the finite element code MARC by Smit [11].

In this chapter these equations will be shortly outlined, without the intention to be complete.

2.1 A one-dimensional model for strain hardening

A one-dimensional model for the strain-hardening behaviour of polymers below their glass transition points has been proposed by Haward and Thackray [5]. The model consists of a Hookean spring in series with an Eyring dashpot and rubber elasticity spring in parallel, as shown in figure 2.1. The model may be used for engineering and true stresses.

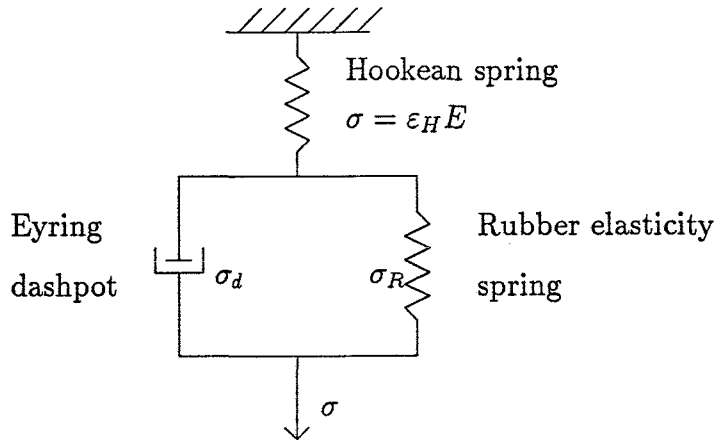

Figure 2.1: The mechanical model according to Haward and Thackray: a Hookean spring in series with an Eyring dashpot and rubber elasticity spring in parallel.

In accordance with figure 2.1 the strain may be written as:

$$\varepsilon = \varepsilon_H + \varepsilon_p \tag{2.1}$$

where ε_H and ε_p are the Hookean and plastic strains respectively, and ε may be defined as:

$$\varepsilon = \frac{l - l_0}{l_0} \tag{2.2}$$

At large strains usually $\varepsilon_p \gg \varepsilon_H$. The Hookean spring predicts with considerable success the initial elastic deformation. The Eyring dashpot predicts with considerable success the strain rate and temperature dependent yield stress. However, the rubber elasticity spring which provides for strain hardening is still the most difficult element to model, and the large strain behaviour is predicted with varying success. Therefore, in section 2.1.1 a short review of the development of one-dimensional rubber elasticity equations will be given, without the intention to be complete.

2.1.1 The rubber elasticity spring

The Langevin equation

According to Treloar [12] the engineering stress in the rubber elasticity spring may be represented by:

$$\sigma_{R(Eng)} = \frac{1}{3} nkT\sqrt{N}\left[\mathcal{L}^{-1}\left(\frac{\lambda_c}{\sqrt{N}}\right) - \lambda_c^{-\frac{3}{2}}\mathcal{L}^{-1}\left(\frac{1}{\sqrt{\lambda_c N}}\right)\right] \tag{2.3}$$

where n is the number of chains per unit volume between points of entanglement, k the Boltzmann constant, T the absolute temperature, N the number of Kuhn lengths between points of entanglement, $\mathcal{L}^{-1}$ the inverse Langevin function, and λ_c the chain stretch. The Langevin function is defined by:

$$\mathcal{L}(\beta) = \coth\beta - \frac{1}{\beta}\,;\ \beta = \mathcal{L}^{-1}\left(\frac{\lambda_c}{\sqrt{N}}\right) \tag{2.4}$$

Equation (2.3) results in asymptotically increasing stress as the chain stress reaches its limiting value $\lambda_{max} = \sqrt{N}$. It is assumed that λ_{max} can never be exceeded even at long times and high stresses. However, according to refs. [5] and [2] the Langevin equation does not perform very well at the highest strains.

The one-dimensional Gaussian equation

In the Gaussian treatment, it is assumed that the polymer chains have a Gaussian distribution and the polymer coils have no limiting ultimate elongation. In uniaxial tension the Gaussian equation is represented by:

$$\sigma_{R(True)} = G_p(\lambda^2 - \frac{1}{\lambda}) \tag{2.5}$$

where G_p is called the strain hardening modulus.

The Rivlin-Mooney equation

In the Rivlin-Mooney theory of rubber elasticity the equation is related to the basic stored energy function. The assumption of a Gaussian distribution of the polymer chains is not invoked. In uniaxial tension the Rivlin-Mooney equation is represented by:

$$\sigma_{R(True)} = 2K_1(\lambda^2 - \frac{1}{\lambda}) + 2K_2(\lambda - \frac{1}{\lambda^2}) \tag{2.6}$$

Since $K_1/K_2 \approx 10$ equation (2.6) is almost identical to equation (2.5). The Rivlin-Mooney equation has been evaluated in several studies, and has shown to agree with experimental results on PVC [2] and LDPE [9].

2.1.2 The plastic deformation

In this section the one-dimensional Gaussian equation (2.5) will be used to derive a formula which relates the engineering stress σ_{Eng} and the natural draw ratio λ_D in the stabilized neck to the strain hardening modulus G_p. Most of the equations and assumptions are proposed by Haward [5,6,7,8]. The visco-plastic deformation may be described as follows:

$$\frac{d(ln\lambda)}{dt} = K_1 \, exp\left(\frac{V\sigma_{d(True)}}{4kT}\right) \tag{2.7}$$

where $\sigma_{d(True)}$ is the true stress in the damper described by the Eyring viscosity function [5], K_1 a constant, V the 'Eyring volume', k the Boltzmann constant and T the absolute temperature. From the mechanical model depicted in figure (2.1), it follows that:

$$\sigma_{d(True)} = \sigma_{True} - \sigma_{R(True)} \tag{2.8}$$

Equation (2.7) can now be rewritten as:

$$\frac{d(ln\lambda)}{dt} = K_1 \, exp \, K_2(\sigma_{True} - \sigma_{R(True)}) \tag{2.9}$$

where $K_2 = V/4kT$. Combination of the Gaussian equation (2.5) for the rubber elasticity spring and equation (2.9) results in:

$$\sigma_{True} = \frac{1}{K_2} ln\left(\frac{1}{K_1}\frac{d(ln\lambda)}{dt}\right) + G_p\left(\lambda^2 - \frac{1}{\lambda}\right) \tag{2.10}$$

$$= Y + G_p\left(\lambda^2 - \frac{1}{\lambda}\right) \tag{2.11}$$

where Y is called the yield stress. Y is only constant under isothermal conditions and if the effect of changing strain rate during a tensile test is neglected. Furthermore, the yield stress normally dominates low strain behaviour and the second term dominates large strain behaviour. The engineering stress is given by:

$$\sigma_{Eng} = \frac{Y}{\lambda} + G_p\left(\lambda - \frac{1}{\lambda^2}\right) \tag{2.12}$$

Necking occurs if:

$$\frac{d\sigma_{Eng}}{d\lambda} < 0 \text{ , while } \lambda \rightarrow 1 \tag{2.13}$$

where:

$$\frac{d\sigma_{Eng}}{d\lambda} = G_p\left(1 + \frac{2}{\lambda^3}\right) - \frac{Y}{\lambda^2} \tag{2.14}$$

and so:

$$Y > 3G_p \tag{2.15}$$

Relation (2.15) broadly determines wether the polymer extends uniformly or necks, and is often mentioned in literature as Considere's condition for necking. In ref. [7] it is proposed that at the natural draw ratio λ_D the engineering stress σ_{Eng} is equal to the yield stress Y and so obtain the equation:

$$\frac{\sigma_{Eng}}{G_p} = \frac{\lambda_D - \frac{1}{{\lambda_D}^2}}{1 - \frac{1}{\lambda_D}} \tag{2.16}$$

The natural draw ratio λ_D is the maximum stretch that can be obtained when the plastic is being drawn from unorientated material. The strain hardening modulus increases with decreasing λ_D and increasing σ_{Eng}. This equation will be applied to experimental engineering stress-strain curves of polycarbonate in order to determine the strain hardening modulus G_p.

2.2 The compressible Leonov model with strain hardening

A compressible Leonov model is implemented in the finite element code MARC by Smit [11]. The strain hardening is modeled by a so-called eight-chain non-gaussian model based on a Langevin function, and a three-dimensional Gaussian equation. From numerical simulations with both strain hardening models it followed that stabilization and propagation of the neck is possible without a strong upsweep of the Langevin equation. The Langevin function in the eight-chain non-gaussian network just resulted in an earlier stabilization of the neck, a higher stress level during neck propagation, and a thicker neck.

2.2.1 The eight-chain non-gaussian model

According to Arruda and Boyce [1], this model was claimed to be able to describe the strain hardening during uniaxial compression and plain strain compression of polycarbonate and polymethylmethacrylate (PMMA). A slightly adjusted model was used by Smit [11] This model assumes that plastic *and* elastic deformation reduces the configural entropy of the system. This implies that the Cauchy stress tensor σ can be decomposed into a hardening stress tensor $\mathbf{W}$ and an effective stress tensor $\mathbf{T}$:

$$\sigma = \mathrm{T} + \mathrm{W} \tag{2.17}$$

The hardening stress tensor $\mathbf{W}$ is given by

$$\mathrm{W} = \frac{1}{3} nkT \frac{N}{\lambda_c} \mathcal{L}^{-1}\left(\frac{\lambda_c}{\sqrt{\mathrm{N}}}\right) \mathrm{B^d} \;\; ; \;\; \lambda_c = \sqrt{\mathrm{tr(B)}/3} \tag{2.18}$$

where n is the number of chains per unit volume between points of entanglement, k the Boltzmann constant, T the absolute temperature, λ_c the chain stretch, N the number of Kuhn lengths between points of entanglement, $\mathcal{L}^{-1}(\lambda_c/\sqrt{\mathrm{N}})$ the inverse Langevin function, and $\mathbf{B}$ the left Cauchy-Green strain tensor.

2.2.2 The three-dimensional Gaussian equation

The Gaussian work hardening function is defined by

$$\mathrm{W} = G_w \mathrm{B}^d \tag{2.19}$$

where $\mathbf{W}$ is the hardening stress tensor as defined in section 2.2.1, and G_w a constant strain hardening modulus.

Chapter 3

Experimental

3.1 Tensile tests

The most stress-strain curves are obtained by stretching a dumbbell-shaped specimen in a tensiometer at a constant rate of extension. The stress is usually calculated by dividing the mean axial load F by the initial cross-sectional area A_0, i.e. the engineering stress σ_{Eng}. The corresponding engineering strain e is calculated by dividing the grip displacement ΔL of the tensiometer by the initial distance L_0 between the grips. Only if the deformation does take place in a uniform manner, the engineering stress σ_{Eng} can easily be transformed into true stress σ_{True} by:

$$\sigma_{True} = \frac{F}{A} = \frac{F}{A_0}\frac{A_0}{A} = \sigma_{Eng}\frac{A_0}{A} \tag{3.1}$$

where A is the current cross-sectional area. If incompressibility is assumed, then the volume remains unchanged and equation (3.1) can be written as:

$$\sigma_{True} = \lambda\sigma_{Eng} \tag{3.2}$$

where $\lambda = L/L_0$ is the extension ratio. However, this test suffers from several disadvantages.

- The true strain rate, defined by $\mathrm{d}\ln\lambda/\mathrm{d}t$ where $\lambda = L/L_0$ is the extension ratio, decreases if λ increases.
- Once the specimen develops a neck, there is no direct correlation between the grip displacement and the local strain or local strain rate due to nonhomogeneous deformation.

Despite these disadvantages this type of tensile testing will be used.

3.2 Material

In the experiments the amorphous polymer polycarbonate (PC) (Lexan) is used, which has a glass transition temperature of 423 K. Flat dumbbell shaped specimens and axisymmetrical dumpbell shaped specimens have been used to investigate the influence of different stress-strain fields on the stress-strain curves. If the stress-strain curves are approximately equal, then the flat specimens can numerically be modeled by axisymmetrical specimens.

The flat dumbbell shaped specimens, about 12 mm wide at the minimum initial cross-sectional area, were machined out of about 2.8 mm thick sheets. These sheets were moulded

at 523 K for 5 minutes under a pressure of 9.6 MN m^{-2} whereafter they are cooled down in a few minutes under the same pressure. Usually, the flat specimen develops a shear band and necks, i.e. the strain is not homogeneous. In order to measure the strain locally, the strain field is made visible by putting a rectangular grid of dots on the surface of the specimens. Ideally, the distance between the dots should be much smaller than the characteristic length of the neck, but much larger than the microscopic deformation domains. Because we are only interested in the draw ratio λ_D in the stabilized neck, a suitable distance between the dots is chosen equal to 2 mm. The grid pattern is obtained by spraying black paint (Spray-Enamel) through a 0.07 mm thick metal plate with 0.2 mm diameter holes spaced 2 mm apart in a rectangular grid pattern.

The axisymmetrical dumbbell shaped specimens are machined on a lathe out of 10 mm diameter extruded rods with a minimum initial diameter equal to 7 mm. Usually, the axisymmetrical specimens also deform not homogeneously, but the draw ratio in the neck is simply related to the decrease in diameter, as will be shown in section 4.2. One specimen is annealed for one hour at a temperature of 413 K in order to investigate the effect on stress level during neck propagation.

Chapter 4

Results

4.1 Tensile tests with flat dumbbell shaped specimens

The flat dumbbell shaped specimens have been tested non-isothermal at three different temperatures and one constant grip velocity, and isothermal at one temperature and two different constant grip velocities. At each combination of strain rate and temperature, at least 4 specimens were used to minimize measurement errors.

The isothermal and non-isothermal tensile tests are performed each by a different tensile machine. This is noted because the accuracy of the load registered by the 'isothermal tensile machine' is very doubtful, in contrast with the 'non-isothermal tensile machine' which registers the load with a relative measurement error of about 0.5 %. The relative measurement error of the cross-sectional area has a value of about 4 % and therefore dominates the measurement error of the stress.

After pulling the specimen to a final elongation the natural draw ratio in the neck should be measured when the specimen is still in the test frame, because the specimen exhibits viscoelastic strain recovery after removal from the test frame. However, the natural draw ratio is then difficult to measure in case of the non-isothermal tensile tests because the specimen is situated in an oven, and impossible to measure in case of the isothermal tensile tests because the specimen is situated in a tube filled with water. Therefore, the natural draw ratio is determined after unloading and removal from the test frame, by measuring the distance between a number of dots located along a few parallel lines.

The strain recovery has a time-dependent viscoelastic nature, therefore the strain recovery depends on the load history, i.e. the hold time period, the grip velocity and time used for unloading, and the time after unloading when the distance between the dots is measured. The time periods used in the tensile tests are approximately one minute, half a minute, and one minute respectively. In case of the non-isothermal tensile tests at room temperature it was possible to estimate the amount of strain recovery. The stress-strain curves, measurement errors, and influence of the paint on the stress-strain curves will be explained more extensively in section 4.1.1 than in other sections.

4.1.1 Non-isothermal tensile tests

The non-isothermal tensile tests were performed at a room temperature of 297 K and in an oven at temperatures of 323 K and 373 K. The constant grip velocity was equal to 5 mm/min and the initial distance L_0 between the grips of the tensiometer was equal to 110

mm, which corresponds to an engineering strain rate with a value equal to about $1 \cdot 10^{-3}$ s^{-1}. All specimens were pulled to a final elongation of 40 mm. The specimens which were tested in the oven were put in the oven 15 minutes before the tensile test was performed, to bring the entire system to thermal equilibrium.

Figure 4.1 shows the engineering stress-strain behaviour of PC for the three different temperatures.

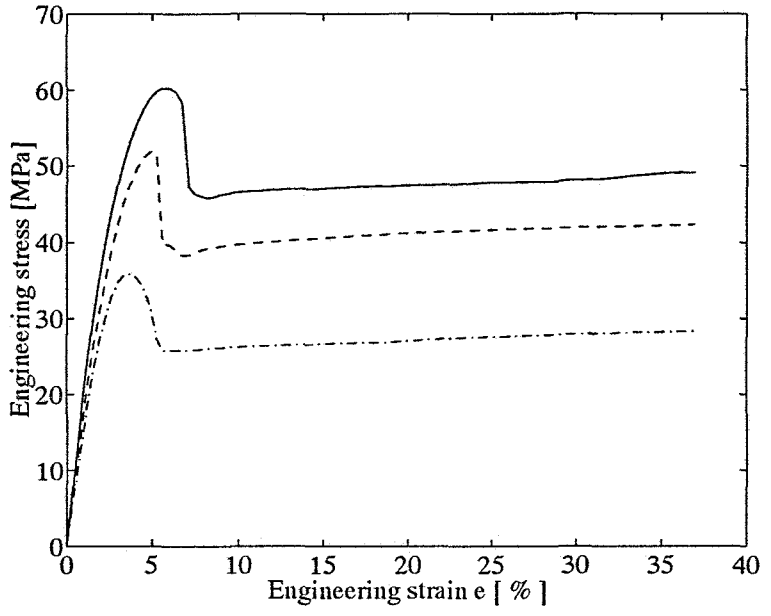

Figure 4.1: Engineering stress-strain curves of PC at temperatures of 297 K (solid), 323 K (- -) and 373 K (- ·).

Polycarbonate exhibits stable necking at all temperatures. At higher temperatures the material becomes more rubber like and the yield point, the strain at the yield point, and the stress during neck propagation decreases.

The specimen deforms uniformly and the load increases monotonically until a maximum is reached at the yield point. At the yield point some part of the specimen must be subjected to a higher stress than the remainder, either because the cross-sectional area is less or because of stress concentrations. The extra stress produces a larger strain and decreases the cross-sectional area of the weak point. Generally, this coincides with the formation of a shear band. The system becomes unstable, a neck is formed and the load drops. The load decreases, because the effect of decreasing cross-sectional area is stronger than the continuously increasing true stress due to strain hardening. In some references, the decreasing load is also partly blamed to true softening, but a solid proof has never been shown so far. If the load drops, then the elastic unloading of the rest of the specimen causes extra heating of the neck, which probably results in a temporary decreasing viscosity and less resistance against deformation. If a stable neck is formed, the shoulders travel along the specimen, which is called 'cold drawing'. The neck propagates at a slightly increasing value of the engineering stress. The sum of the velocities of the travelling shoulders is almost equal to the grip displacement, because the remainder of the specimen has a local strain rate almost equal to zero. Therefore, the local strain rate in the travelling shoulder is much larger than the engineering strain rate.

In table 4.1 the yield stress σ_y, the stress σ_{end} at the end of the tensile test, the after unloading measured natural draw ratio λ_D, and the strain hardening modulus G_p are shown, for the three temperatures used.

Table 4.1: Numerical results from the non-isothermal tensile tests

T [K]	σ_y [MN·m^{-2}]	σ_{end} [MN·m^{-2}]	λ_D [-]	G_p [MN·m^{-2}]
297	59.93	48.30	1.67	14.6
323	52.29	42.18	1.71	12.6
373	35.01	27.32	1.71	8.3

The strain hardening modulus G_p is calculated with equation (2.16), where $\sigma_{Eng} = \sigma_{end}$. The stress σ_{end} is much more sensitive to a decreasing temperature than the natural draw ratio, therefore the decrease of G_p is dominated by σ_{end}. At higher temperatures the natural draw ratio slightly increases, as expected. However, the third decimal of the natural draw ratio already suffers from measurement errors (± 2). The relative measurement error in G_p is equal to about 7%.

In case of the non-isothermal tensile test at room temperature it was possible to estimate the natural draw ratio when the specimen was still in the test frame: $\lambda_D = 1.79$. This means that the amount of strain recovery was equal to about 7% one minute after unloading. One specimen was subjected to a 'hold time' of 30 minutes, which resulted in a strain recovery of about 5%. A relative error in λ_D of 6% (λ_D=1.7 instead of 1.8) results in a relative error of 2% in G_p. Therefore, the total relative measurement error in G_p is approximately 9%. Two specimens without a grid of dots were tested at room temperature. It appeared that the paint had no significant influence on the stress-strain curves.

4.1.2 Isothermal tensile tests

The isothermal tensile tests were performed in water with a temperature of 296 K. The initial distance L_0 between the grips of the tensiometer was equal to 108 mm, and the two different grip velocities were equal to 5 mm/min and 500 mm/min, which corresponds to engineering strain rates with values equal to about $1{\cdot}10^{-3}$ s^{-1} and $1{\cdot}10^{-1}$ s^{-1} respectively. All specimens were pulled to a final elongation of 40 mm. The load recorded by the tensile machine was not very accurate, but the engineering stress is still given in table 4.2.

Table 4.2: Numerical results from the isothermal tensile tests with PC

$\dot{\varepsilon}$ [s^{-1}]	σ_y [MN·m^{-2}]	σ_{end} [MN·m^{-2}]	λ_D [-]	G_p [MN·m^{-2}]
$1{\cdot}10^{-3}$	59.39	50.06	1.67	15.2
$1{\cdot}10^{-1}$	61.67	54.23	1.71	16.5

The natural draw ratio increases with increasing strain rate, and the natural draw ratio at a strain rate of $1{\cdot}10^{-3}$ is equal to the corresponding 'non-isothermal natural draw ratio' of table 4.1.

4.2 Tensile tests with axisymmetrical dumbbell shaped specimens

Three axisymmetrical dumbbell shaped specimens have been tested non-isothermal at a room temperature of 297 K. One of them was annealed for one hour at a temperature of 413 K, i.e. 10 K under the glass transition temperature. The initial distance L_0 between the grips of the tensiometer was equal to 70 mm, and the grip velocity was equal to 5.2 mm/min, which corresponds to an engineering strain rate with a value equal to about $1{\cdot}10^{-3}$ s^{-1}. Because of uniaxial tension the draw ratio in the neck is related to the diameter of the neck by the following equation:

$$\lambda_D = \left(\frac{D}{D_0}\right)^{-2} \tag{4.1}$$

The engineering stress-strain curves are depicted in figure 4.2.

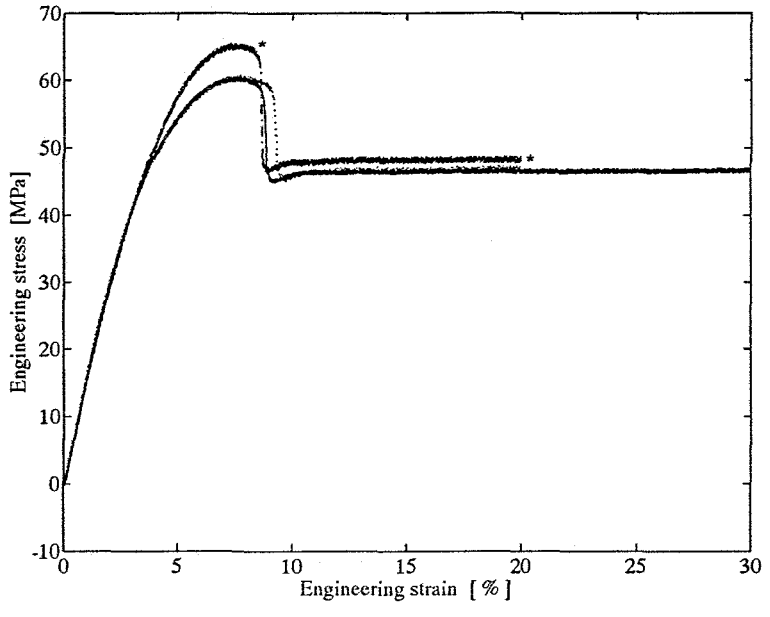

Figure 4.2: Engineering stress-strain curves of axisymmetrical specimens. One specimen (*) was annealed

In table 4.3 the yield stress σ_y, the stress σ_{end} at the end of the tensile test, the natural draw ratio λ_D after unloading, and the strain hardening modulus G_p are shown.

Table 4.3: Tensile test results from the annealed (case 1), and not annealed (case 2) axisymmetrical specimens.

case	σ_y [MN·m^{-2}]	σ_{end} [MN·m^{-2}]	λ_D [-]	G_p [MN·m^{-2}]
1	65.55	48.23	1.74	14.55
2	60.68	46.80	1.74	14.12

Annealing of the specimen results in a higher yield stress, but in an approximately equal

stress during neck propagation compared to the not annealed specimens. This could be an indication for true strain softening. Comparing the not annealed axisymmetrical specimens with the flat specimens, σ_y and σ_{end} are almost the same, and λ_D is slightly increased. Therefore it is allowed to model both type of specimens with axisymmetrical elements in the finite element code MARC.

4.3 Finite element simulations with the compressible Leonov model

In this chapter finite element simulations will be performed, based on a compressible Leonov model with Gaussian strain hardening developed by Smit [11]. Uniaxial tension of axisymmetric bars will be considered. The model is already briefly outlined in section N, but some further remarks are necessary:

- The model as used by Smit did not contain a pressure dependent viscosity or an intrinsic softening effect (softening immediately after yield).
- Thermo-coupled (heat by viscoplastic work) and isothermal analyses can be performed.
- Gaussian strain hardening is assumed because G_w in equation (2.19) is very similar to G_p in the one-dimensional Gaussian equation (2.5).

It would be very interesting if the calculated value for G_p, by applying equation (2.16) to the numerical stress-strain curves, would be equal to the value of G_w used in the numerical simulations. The numerical stress-strain curves will be compared to the experimental stress-strain curves of section 4.1 and 4.2, especially the yield stress and the stress during neck propagation. The deflections between these curves are tried to be minimized by varying the strain hardening modulus G_w and by introducing a pressure dependent viscosity η defined by:

$$\eta = \frac{A\sqrt{\frac{1}{2}II_{\mathbf{T}^d}}}{\sinh\left[\frac{1}{\tau_0}\left(\sqrt{\frac{1}{2}II_{\mathbf{T}^d}} - \sqrt{\frac{3}{2}}p\mu\right)\right]} \tag{4.2}$$

where A is a time constant, $II_{\mathbf{T}^d}$ the second invariant of the deviatoric stress, τ_0 a characteristic stress, and p the hydrostatic pressure defined by

$$A = A^* e^{\frac{\Delta U}{RT}} \tag{4.3}$$

$$II_{\mathbf{T}^d} = \mathbf{T}^d : \mathbf{T}^d \tag{4.4}$$

$$\tau_0 = RT/V^* \tag{4.5}$$

$$p = -\frac{1}{3}tr(\sigma) \tag{4.6}$$

in which A^* is a constant pre-exponential factor, ΔU an enthalpy barrier, R the gas constant, T the absolute temperature, V^* the 'Eyring volume', and μ a pressure sensitivity factor.

4.3.1 Specimen geometry and material parameters

A hour-glass shaped axisymmetrical bar is used, as shown in figure 4.3. The bar has a small initial cosine shaped imperfection defined by:

$$R_{0_i}(z) = R_0 \left[1 - \frac{1}{2}(1 - \sqrt{\alpha})(1 - \cos(\pi z/\beta R_0))\right] \quad \text{for } 0 \leq z \leq \beta R_0 \tag{4.7}$$

where R_0 is the initial radius, $\alpha = R_{0_i}^2(0)/R_0^2$ is the relative cross sectional area of the bar, and β controls the imperfection length.

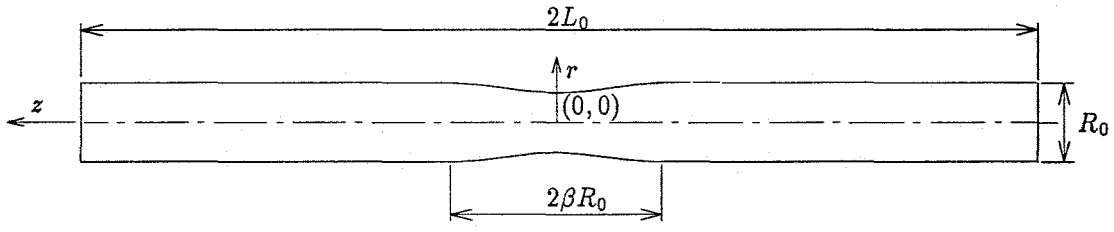

Figure 4.3: Analytical model of the axisymmetrical test specimen.

The values of the geometrical parameters used are L_0=120 mm, R_0=3 mm, $\alpha = 0.97$, and $\beta = 1$. Because of symmetry, only a quarter of the specimen is modeled in the finite element code MARC. The values of the material parameters used are: $E = 2400$ MPa, ν=0.35, $A^* = 3.8568 \cdot 10^{-27}\text{s}^{-1}$, $V^* = 3.6453 \cdot 10^{-4}\text{m}^3/\text{mol}$, $\Delta U = 2.617 \cdot 10^{-5}\text{J/mol}$. If a pressure dependent viscosity is assumed then $\mu = 0.051$, otherwise $\mu = 0$. The initial specimen temperature and initial environmental temperature are chosen equally.

4.3.2 Simulations with a pressure independent viscosity

Non-isothermal simulations are performed with an engineering strain rate of $1{\cdot}10^{-3}$ s^{-1}, and initial temperatures of 297 K and 323 K. The values used for G_w in equation (2.19) are equal to 12.08 (also used by Smit [11]), 13.4, and 15.2. The engineering stress-strain curves, and the strain hardening modulus G_p versus engineering strain curves are depicted in figure 4.4 (T=294 K) and figure 4.5 (T=323 K). G_p is calculated by applying equation (2.16) to the stress-strain curves, where λ_D is calculated at z=0 (figure 4.3).

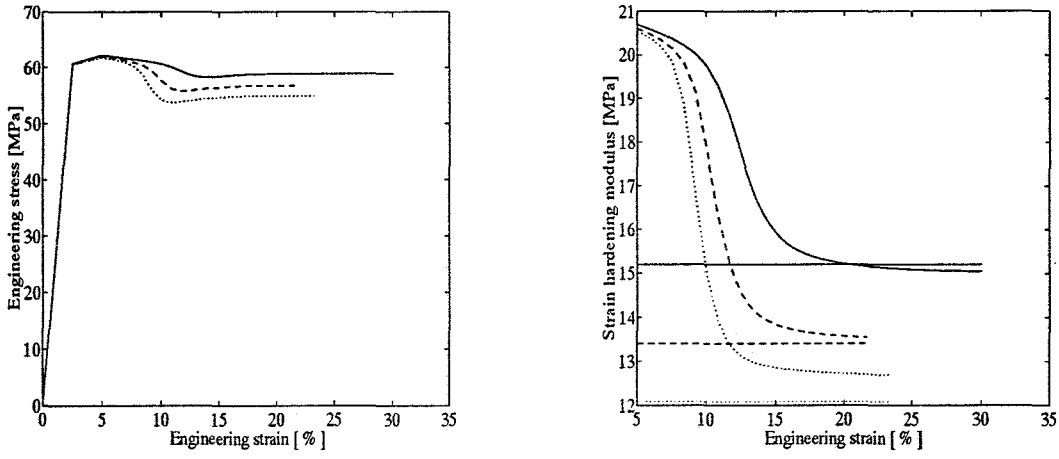

Figure 4.4: Engineering stress-strain curves (left), and strain hardening modulus G_p versus engineering strain curves (right), at a temperature of 297 K. The values of G_w used in the compressible Leonov model are: G_w = 12.08 (··), 13.4 (- -), 15.2 (solid)).

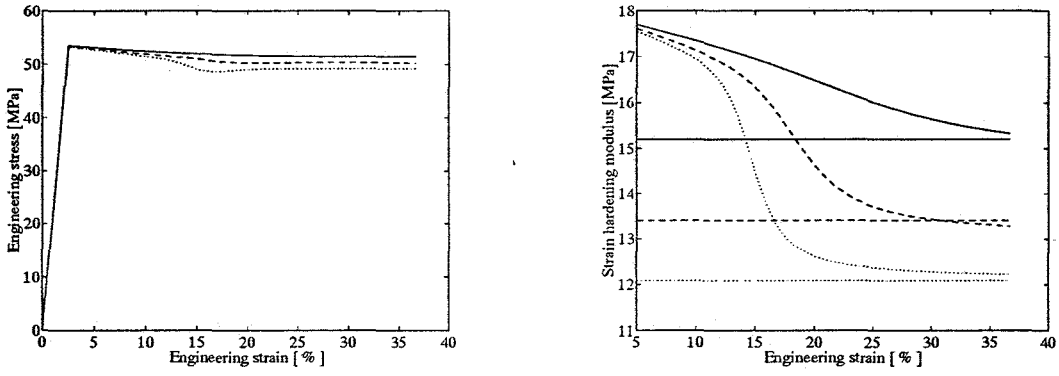

Figure 4.5: Engineering stress-strain curves (left), and strain hardening modulus G_p versus engineering strain curves (right), at a temperature of 323 K. The values of G_w used in the compressible Leonov model are: G_w = 12.08 (··), 13.4 (- -), and 15.2 (solid).

Although equation (2.16) i s a quite simple equation, derived from a simple one-dimensional and slightly different constitutive model, it is capable of approaching the strain hardening modulus G_w used in the compressible Leonov model. At a higher temperature (323 K), the neck needs more time to stabilize. The neck is considered to be stabilized if G_p is approximately constant. Comparing the stress-strain curves of figure 4.4 and figure 4.5 to the experimental stress-strain curves of figure 4.1, it can be concluded that the yield stress is predicted with considerable success, but the stress level during neck propagation is still to high. It is very clear that the strain hardening dominates the large strain behaviour; the stress level during neck propagation decreases at lower values of the strain hardening modulus G_w. However, it was not possible to approach the experimental stress levels because lower values

of G_w caused numerical problems. These numerical problems resulted in different engineering strains at the end of the simulations. In order to be able to compare the results of the numerical simulations, the values of σ, λ_D, and G_p are shown in table 4.4 at an engineering strain of 21.7%. The natural draw ratio is in most of the simulations larger and has a wider range than in the experiments. In contrast with the experiments , λ_D decreases at higher temperatures.

Table 4.4: Numerical results from the finite element simulations at temperatures of 297 K and 323 K, an engineering strain of 21.7%, and a pressure independent viscosity ($\mu = 0$).

T [K]	G_w [MN·m^{-2}]	σ_y [MN·m^{-2}]	σ [MN·m^{-2}]	λ_D [-]	G_p [MN·m^{-2}]
297	12.08	61.76	54.95	2.992	12.70
297	13.40	61.96	56.76	2.839	13.54
297	15.20	62.22	58.87	2.481	15.16
323	12.08	53.29	49.16	2.544	12.49
323	13.40	53.38	50.26	2.063	14.17
323	15.20	53.51	51.64	1.497	16.32

4.3.3 Simulations with a pressure dependent viscosity

Non-isothermal simulations are performed with an engineering strain rate of $1{\cdot}10^{-3}$ s^{-1}, and an initial temperature of 323 K, but now with a pressure dependent viscosity. Introducing a pressure dependent viscosity results in a lower viscosity and therefore in a lower stress level and a higher natural draw ratio. The values used for G_w in equation (2.19) are equal to 12.08, 13.4, and 15.2. The engineering stress-strain curves, and the strain hardening modulus G_p versus engineering strain curves are depicted in figure 4.6.

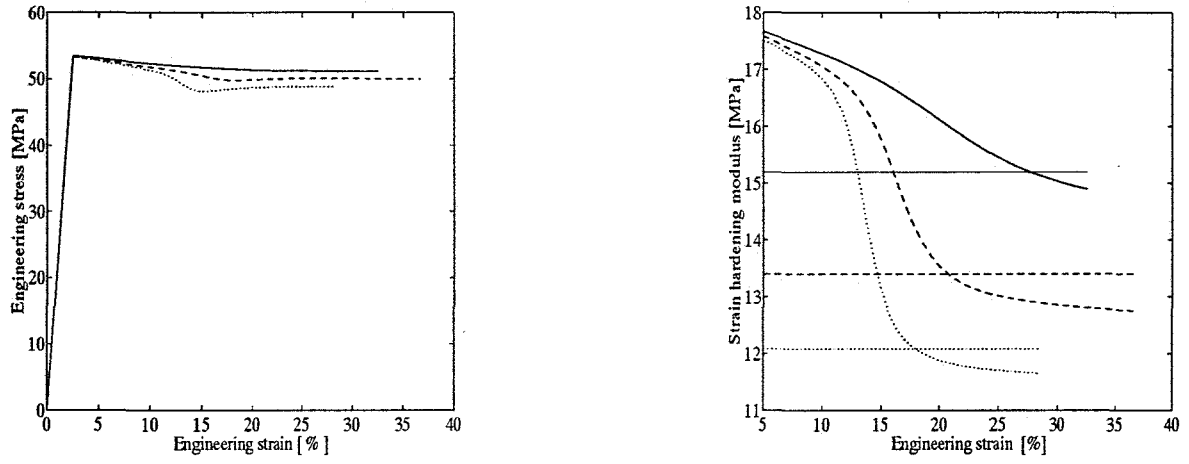

Figure 4.6: Engineering stress-strain curves (left), and strain hardening modulus G_p versus engineering strain curves (right), at a temperature of 323 K, but now with a pressure dependent viscosity. The values of G_w used in the compressible Leonov model are: $G_w = 12.08$ (··), 13.4 (--), 15.2 (solid).

The decrease in stress level is not sufficient to approach the experimental stress level of figure 4.1. In table 4.5 the numerical results from the finite element simulations based on a pressure dependent viscosity are shown, together with the numerical results of section 4.3.2 (pressure independent viscosity).

Table 4.5: Numerical results from the finite element simulations at a temperature of 323 K, an engineering strain of 21.7%, and a:
- pressure independent viscosity ($\mu = 0$)
- pressure dependent viscosity ($\mu = 0.051$).

μ [-]	G_w [MN·m^{-2}]	σ_y [MN·m^{-2}]	σ [MN·m^{-2}]	λ_D [-]	G_p [MN·m^{-2}]
0.000	12.08	53.29	49.16	2.544	12.49
0.051	12.08	53.27	48.76	2.773	11.80
0.000	13.40	53.38	50.26	2.063	14.17
0.051	13.40	53.36	49.98	2.340	13.27
0.000	15.20	53.51	51.64	1.497	16.32
0.051	15.20	53.48	51.30	1.609	15.88

A disadvantage of the pressure dependent viscosity is the higher natural draw ratio. In order to decrease the stress during neck propagation, true strain softening should be implemented in the compressible Leonov model.

Chapter 5

Conclusions and recommendations

5.1 Conclusions

- Experimental:
  - From applying the one-dimensional equation (2.16) to the experimental stress-strain curves of polycarbonate, it follows that the strain hardening modulus G_p decreases at higher temperatures and lower strain rates.

- Compressible Leonov model:
  - Although equation (2.16) is a quite simple equation, it is capable of approaching the strain hardening modulus G_w used in the compressible Leonov model.
  - It is not possible to fit the large strain behaviour of the compressible Leonov model, i.e. the stress during neck propagation and the natural draw ratio, on the experimental data, by introducing a pressure dependent viscosity or by varying the strain hardening modulus G_w in the numerical simulations which are performed.

5.2 Recommendations

- Experimental:
  - A computer-aided video extensometer should be used, which analyses the grid pattern in real time if flat specimens are used. If axisymmetrical specimens are used, the diameter of the neck should be analyzed.
  - A larger range of the natural draw ratio λ_D should be investigated

- Compressible Leonov model
  - In order to decrease the stress during neck propagation, true strain softening should be implemented.

Bibliography

[1] Arruda, E.M., Boyce, M.C., 'Evolution of plastic anisotropy in amorphous polymers during finite straining', *Int. J. Plasticity*, Vol. 9, pp. 697-720, 1993.

[2] Cross, A., and Haward, R.N., 'Orientation hardening of PVC', *Polymer*, Vol. 19, pp. 677-682, 1978, and Vol. 21, pp. 1226, 1980.

[3] G'Sell, C., and Jonas, J.J., 'Yield and transient effects during the plastic deformation of solid polymers', *J. Mater. Sci.*, Vol. 16, pp. 1956-1974, 1981.

[4] G'Sell, C., Hiver, J.M., Dahoun, A., and Souahi, A., 'Video-controlled tensile testing of polymers and metals beyond the necking point', *J. Mater. Sci.*, Vol. 27, pp. 5031-5039, 1992.

[5] Haward, R.N., and Thackray, G., 'The use of a mathematical model to describe isothermal stress-strain curves in glassy thermoplastics', *Proc. Roy. Soc.*, A302, pp. 453-472, 1968.

[6] Haward, R.N., 'The application of a simplified model for the stress-strain curves of polymers', *Polymer*, Vol. 28, pp. 1485-1488, 1987.

[7] Haward, R.N., 'Strain Hardening of Thermoplastics', *Macromolecules*, Vol. 26, pp. 5860-5869, 1993.

[8] Haward, R.N., 'Developments in the study of large deformations of thermoplastics', *94th International Conferance on Deformation, Yield and Fracture of Polymers*, Churchill College, Cambridge, UK, pp. P94/1-P94/4, 1994.

[9] Mills, P.J., Hay, J.N., and Haward, R.N., 'The post-yield behaviour of low-density polyethylenes', *J. Mater. Sci.*, Vol. 20, pp. 501-507, 1985.

[10] Nied, H.F. and Stokes, V.K., and Ysseldyke, D.A., 'High-Temperature Large-Strain Behaviour of Polycarbonate, Polyetherimide and Poly(butylene Terephthalate)', *Pol. Eng. and Sci.*, Vol. 27, pp. 101-107, 1987.

[11] Smit, R.J.M., 'Numerical Simulation of Localization Phenomena in Polymer Glasses', Graduate report TUE WFW 94.046, Eindhoven University of Technology, 1994.

[12] Treloar, L.R.G., 'The Physics of Rubber Elasticity', 2nd Edn, Oxford Univ. Press, 1958.

Appendix A

Extra measurement data

Table A.1: Macrolon plate (PC), non-isothermal, engineering strain rate is equal to about $1{\cdot}10^{-3}\,s^{-1}$.

T [K]	σ_y [MN·m^{-2}]	σ_{end} [MN·m^{-2}]	λ_D [-]	G_p [MN·m^{-2}]
297	62.35	50.24	1.64	15.5

Table A.2: Macrolon plate (PC), isothermal at a temperature of 297 K and two different engineering strain rates.

$\dot{\varepsilon}$ [s^{-1}]	σ_y [MN·m^{-2}]	σ_{end} [MN·m^{-2}]	λ_D [-]	G_p [MN·m^{-2}]
$1{\cdot}10^{-3}$	73.88	61.32	1.64	18.9
$1{\cdot}10^{-1}$	74.61	66.57	1.68	20.3

Table A.3: Injection moulded PC (Lexan), non-isothermal, engineering strain rate is equal to about $1{\cdot}10^{-3}\,s^{-1}$.

T [K]	σ_y [MN·m^{-2}]	σ_{end} [MN·m^{-2}]	λ_D [-]	G_p [MN·m^{-2}]
297	56.61	45.01	1.64	13.9
323	49.42	39.56	1.60	12.3
373	33.31	26.07	1.61	8.1

The stresses in table A.2 are very inaccurate, as noted earlier in section 4.1.2.